arXiv:2508.19544v1 [cs.CV] 27 Aug 2025

WEBEYETRACK: Scalable Eye-Tracking for the Browser via On-Device Few-Shot Personalization

Eduardo Davalos[1*], Yike Zhang[2*], Namrata Srivastava[3], Yashvitha Thatigotla[3], Jorge A. Salas[3], Sara McFadden[3], Sun-Joo Cho[3], Amanda Goodwin[3], Ashwin TS[3], Gautam Biswas[3]

[1]Trinity University, San Antonio, TX, USA
[2]St. Mary's University, San Antonio, TX, USA
[3]Vanderbilt University, Nashville, TN, USA
davalosedu515@trinity.edu, yzhang5@stmarytx.edu, namrata.srivastava@vanderbilt.edu, yashvitha.thatigotla@vanderbilt.edu, jorge.a.salas@vanderbilt.edu, sara.mcfadden@vanderbilt.edu, sj.cho@vanderbilt.edu, ashwindixit9@gmail.com, amanda.goodwin@vanderbilt.edu, gautam.biswas@vanderbilt.edu

Abstract

With advancements in AI, new gaze estimation methods are exceeding state-of-the-art (SOTA) benchmarks, but their real-world application reveals a gap with commercial eye-tracking solutions. Factors like model size, inference time, and privacy often go unaddressed. Meanwhile, webcam-based eye-tracking methods lack sufficient accuracy, in particular due to head movement. To tackle these issues, we introduce **WebEyeTrack**, a framework that integrates lightweight SOTA gaze estimation models directly in the browser. It incorporates model-based head pose estimation and on-device few-shot learning with as few as nine calibration samples ($k \leq 9$). WebEyeTrack adapts to new users, achieving SOTA performance with an error margin of 2.32 cm on GazeCapture and real-time inference speeds of 2.4 milliseconds on an iPhone 14. Our open-source code is available at https://github.com/RedForestAi/WebEyeTrack.

Code — https://github.com/RedForestAI/WebEyeTrack
Website — https://redforestai.github.io/WebEyeTrack/

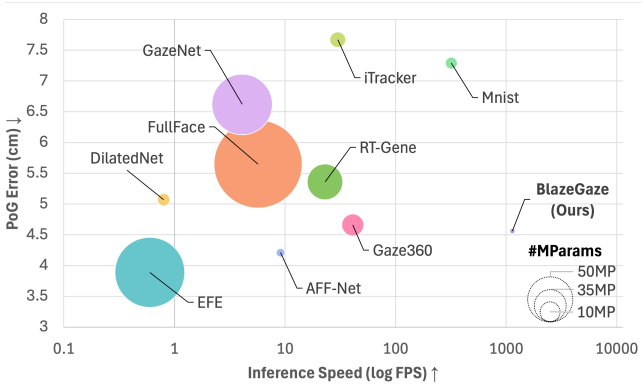

Figure 1: **Point-of-Gaze (PoG) Error (cm) vs. Inference Speed (log-scale FPS) Across Gaze Estimation Methods**: BlazeGaze (ours) achieves high accuracy with orders of magnitude faster inference speed using lightweight CNN BlazeBlocks.

1 Introduction

Eye-tracking has been a transformative tool for investigating human-computer interactions, as it uncovers subtle shifts in visual attention (Jacob and Karn 2003). However, its reliance on expensive specialized hardware, such as EyeLink 1000 and Tobii Pro Fusion has confined most gaze-tracking research to controlled laboratory environments (Heck, Becker, and Deutscher 2023). Similarly, virtual reality solutions like the Apple Vision Pro remain financially out of reach for widespread use. These limitations have hindered the scalability and practical application of gaze-enhanced technologies and feedback systems.

To reduce reliance on specialized hardware, researchers have actively pursued webcam-based eye-tracking solutions that utilize built-in cameras on consumer devices. Two key areas of focus in this field are appearance-based gaze estimation and webcam-based eye-tracking, both of which have made significant advancements using standard monocular cameras (Cheng et al. 2021). For example, recent appearance-based methods have shown improved accuracy on commonly used gaze estimation datasets such as MPIIGaze (Zhang et al. 2015), MPIIFaceGaze (Zhang et al. 2016), and EyeDiap (Alberto Funes Mora, Monay, and Odobez 2014). However, many of these AI models primarily aim to achieve state-of-the-art (SOTA) performance without considering practical deployment constraints. These constraints include varying display sizes, computational efficiency, model size, ease of calibration, and the ability to generalize to new users. While some efforts have successfully integrated gaze estimation models into comprehensive eye-tracking solutions (Heck, Becker, and Deutscher 2023), achieving real-time, fully functional eye-tracking systems remains a considerable technical challenge. Retrofitting existing models that do not address these design considerations often involves extensive optimization and may still fail to meet practical requirements. As a result, state-of-the-art gaze estimation methods have not yet been broadly imple-

*These authors contributed equally.
Copyright © 2025, Association for the Advancement of Artificial Intelligence (www.aaai.org). All rights reserved.

mented, mainly due to the difficulties of running these AI models on resource-constrained devices.

At the same time, webcam-based eye-tracking methods have taken a practical approach, addressing real-world deployment challenges (Heck, Becker, and Deutscher 2023). These solutions are often tied to specific software ecosystems and toolkits, hindering portability to platforms such as mobile devices or web browsers. As web applications gain popularity for their scalability, ease of deployment, and cloud integration (Shukla et al. 2023), tools like WebGazer (Papoutsaki et al. 2016) have emerged to support eye-tracking directly within the browser. However, many browser-friendly approaches rely on simple statistical or classical machine learning models (Heck, Becker, and Deutscher 2023), such as ridge regression (Xu et al. 2015) or support vector regression (Papoutsaki et al. 2016), and avoid 3D gaze reasoning to reduce computational load. While these techniques improve accessibility, they often compromise accuracy and robustness under natural head motion.

To bridge the gap between high-accuracy appearance-based gaze estimation methods and scalable webcam-based eye-tracking solutions, we introduce WEBEYETRACK, a few-shot, headpose-aware gaze estimation solution for the browser (Fig 2). WEBEYETRACK combines model-based headpose estimation (via 3D face reconstruction and radial procrustes analysis) with BlazeGaze, a lightweight CNN model optimized for real-time inference. It computes the Point-of-Gaze (PoG), detects eye state (open/closed) via the eye aspect ratio (EAR) (Soukupová 2016) to suppress predictions during blinks, implements continuous clickstream calibration, and provides online fixation detection via WebFixRT[1], thereby creating a full-featured and web-friendly eye-tracking system. We provide both Python and client-side JavaScript implementations to support model development and seamless integration into research and deployment pipelines. In evaluations on standard gaze datasets, WEBEYETRACK achieves comparable SOTA performance and demonstrates real-time performance on mobile phones, tablets, and laptops.

Overall, our work makes the following contributions:

- WEBEYETRACK: an open-source novel browser-friendly framework that performs few-shot gaze estimation with privacy-preserving on-device personalization and inference.
- A novel model-based metric headpose estimation via face mesh reconstruction and radial procrustes analysis.
- BlazeGaze: A novel, 670KB CNN model based on BlazeBlocks that achieves real-time inference on mobile CPUs and GPUs.

2 Background

Gaze Estimation Classical gaze estimation relied on model-based approaches for (1) 3D gaze estimation (predicting gaze direction as a unit vector), and (2) 2D gaze estimation (predicting gaze target on a screen). These methods used predefined eyeball models and extensive calibration procedures (Dongheng Li, Winfield, and Parkhurst 2005; Wood and Bulling 2014; Brousseau, Rose, and Eizenman 2018; Wang and Ji 2017). In contrast, modern appearance-based methods require minimal setup and leverage deep learning for improved robustness (Cheng et al. 2021).

The emergence of CNNs and datasets such as MPIIGaze (Zhang et al. 2015), GazeCapture (Krafka et al. 2016), and EyeDiap (Alberto Funes Mora, Monay, and Odobez 2014) has led to the development of 2D and 3D gaze estimation systems capable of achieving errors of 6–8 degrees and 3–7 centimeters (Zhang et al. 2015). Key techniques that have contributed to this progress include multimodal inputs (Krafka et al. 2016), multitask learning (Yu, Liu, and Odobez 2019), self-supervised learning (Cheng, Lu, and Zhang 2018), data normalization (Zhang, Sugano, and Bulling 2018), and domain adaptation (Li, Zhan, and Yang 2020). More recently, Vision Transformers have further enhanced accuracy, reducing error to 4.0 degrees and 3.6 centimeters (Cheng and Lu 2022). Despite strong within-dataset performance, generalization to unseen users remains poor (Cheng et al. 2021). Few-shot learning addresses this by adapting to new users with minimal labeled data. However, the few-shot FAZE framework (Park et al. 2019) requires substantial computational resources, including a powerful GPU for real-time inference, while SAGE (He et al. 2019) is a closed-source implementation, restricting evaluation, usage, and practical adoption.

Metric Head Pose Estimation Head pose is frequently utilized to improve gaze estimation (Zhang et al. 2016), but most methods rely on having access to ground-truth poses obtained from depth sensors or multi-camera setups (Alberto Funes Mora, Monay, and Odobez 2014; Sugano, Matsushita, and Sato 2014). These setups are often impractical for browser-based applications. Monocular methods tend to struggle with real-time performance and often produce scale-ambiguous poses (Kazemi and Sullivan 2014; Guo et al. 2021; Baltrusaitis et al. 2018), which renders self-consistent head pose estimation unreliable.

Webcam-based Eye-Tracking Deploying deep learning-based gaze systems in real-world applications is challenging due to high hardware requirements and compatibility issues with programming languages. Most implementations, such as OpenGaze (Zhang, Sugano, and Bulling 2019) and FAZE (Park et al. 2019), are based on C++ and Python and require PyTorch and CUDA, which impose high computational demands unsuited to many consumer devices. Web-compatible tools like iTracker (Krafka et al. 2016) and iMon (Huynh, Balan, and Ko 2021) are often outdated or poorly documented. Additionally, using cloud-based training and inference raises concerns about privacy and latency (Park, Park, and Cha 2021).

Browser-based and Real-time Eye-Tracking Browser-compatible solutions such as RealEye (Pietrzak et al. 2025), WebET (iMotions 2023), and GazeCloudAPI are closed-source and do not provide transparent benchmarking. Among open-source tools, WebGazer (Papoutsaki et al.

[1]https://github.com

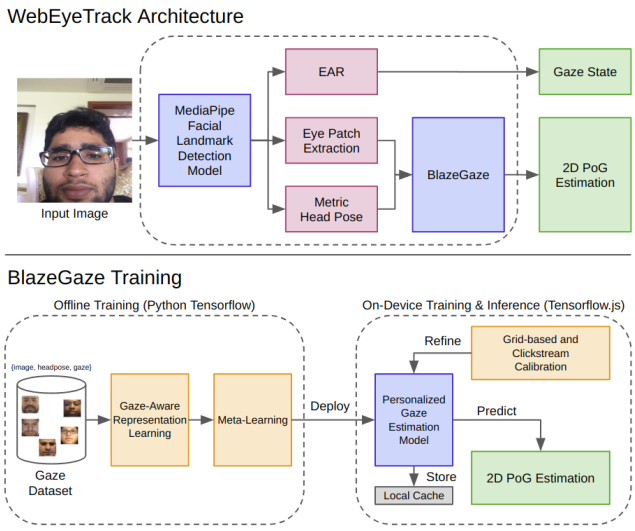

Figure 2: **WEBEYETRACK Framework Overview**: Framework composed of multiple model-based routines along with a CNN-based BlazeGaze gaze estimation model. The BlazeGaze model is trained to ensure privacy with on-device calibration and inference.

2016) is widely used, utilizing facial landmarks and ridge regression for estimating 2D PoG. However, its accuracy declines significantly over time due to its lack of head pose awareness, resulting in the error increasing from approximately 5 to 10 cm during a 20-minute test (Papoutsaki et al. 2018).

We bridge this gap by integrating fast CNN-based gaze estimation, inspired by BlazeFace's BlazeBlocks (Bazarevsky et al. 2019), with meta-learning for few-shot adaptation and real-time inference. Our model is also headpose-aware, improving robustness across users and environments.

3 Method

This section discusses WEBEYETRACK, a real-time gaze estimation framework designed to function effectively in challenging, real-world environments, such as web browsers and mobile devices. As shown in Fig. 2, the computational pipeline consists of utilizing MediaPipe's facial landmark detection model to estimate the gaze state (open/close), eye patch region, and metric head pose. These variables are then passed to BlazeGaze, a lightweight 2D PoG estimation model. A two-step training process is used to derive an adaptive gaze meta-learner that is then deployed to user's browsers and perform on-device calibration, inference, and model caching. We aim to deliver personalized, head-pose-aware gaze predictions with low computational costs.

To accomplish this, WEBEYETRACK incorporates two main components: (1) a model-based 3D face reconstruction pipeline that accurately estimates head pose in metric space from monocular images, and (2) an appearance-based gaze estimation model called BlazeGaze, which utilizes model-agnostic meta-learning (MAML) to adapt to new users with minimal calibration data. This hybrid approach allows our system to use explicit geometric cues (such as head orientation and position) in conjunction with implicit appearance features (like eye-region encoding), resulting in improved generalization and personalization.

We first describe our novel metric 3D face reconstruction and headpose pipeline in Sec. 3.1. This approach leverages MediaPipe's real-time Facial Landmark Detection model and an iris-based depth estimation algorithm to produce a fully metric head pose. We then detail the BlazeGaze model, which adopts a few-shot adaptation approach to learn a user-specific gaze regressor using only a handful of calibration samples ($k \leq 9$), in Sec. 3.2.

3.1 Metric Face Reconstruction and Headpose

3D face reconstruction is used to estimate head pose (position and orientation) in metric space rather than relative units. MediaPipe's Facial Landmark Detection model (Grishchenko et al. 2020) offers a lightweight pipeline for detecting 3D facial landmarks and reconstructing a canonical face mesh. The output UVZ landmark coordinates $\{x_i^I\}_{i=1}^N$ contain X and Y values normalized to screen space, while Z values are relative and scaled using a weak perspective projection. The model also provides a relative face transformation matrix $P = [R \mid t]$, where $R \in \mathbb{R}^{3\times3}$ rotation matrix and $t \in \mathbb{R}^3$ translation vector transform the points from the canonical face coordinate space (FCS) to the camera coordinate space (CCS). The canonical mesh follows a fixed 468-point topology used for consistent face landmark estimation across frames.

In gaze-estimation datasets such as GazeCapture (Krafka et al. 2016), the camera intrinsics are provided, which include the focal length (f_x, f_y) along with the principal point (c_x, c_y). This supports the construction of a camera intrinsics matrix:

$$K = \begin{bmatrix} f_x & 0 & c_x \\ 0 & f_y & c_y \\ 0 & 0 & 1 \end{bmatrix} \tag{1}$$

The first step is the conversion of facial landmarks from UVZ in image-plane space to XYZ space through reprojection, leveraging the camera intrinsics matrix:

$$X = \frac{(u - c_x) \cdot z}{f_x}, \quad Y = \frac{(v - c_y) \cdot z}{f_y} \tag{2}$$

To convert all 2D UVZ facial landmarks into 3D XYZ space, we reproject and normalize the points (centered around the nose [ID=4] and with face width set to 1 with leftmost [ID=356] and rightmost [ID=127] landmarks) using the following:

$$\{x_i^R\}_{i=1}^N = \text{Reproject}(\{x_i^I\}_{i=1}^N, K') \tag{3}$$

$$x_i^F = \frac{x_i^R - x_{nose}^R}{\|x_{left}^R - x_{right}^R\|} \tag{4}$$

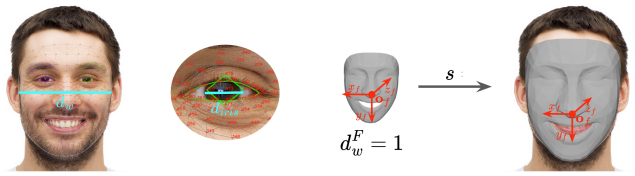

Figure 3: **Iris-based Face Scaling**: A constant iris diameter α enables metric face width estimation, which is applied to the normalized face mesh to approximate the user's true facial dimensions.

Face Scale Estimation The normalized XYZ facial landmarks $\{x_i^F\}_{i=1}^N$ are unitless and relative, making them unsuitable for downstream tasks due to inconsistent depth scaling. To recover metric position and orientation (in centimeters), we first estimate face scale. Using a standard iris diameter of $\alpha = 1.2$ cm from gaze estimation literature (Wen et al. 2020), we compute face width from the pixel ratio between the iris diameter d_{iris}^I to face width d_w^I. This ratio allows transforming the normalized points into metric landmarks $\{x_i^{F'}\}_{i=1}^N$ via:

$$\{x_i^{F'}\}_{i=1}^N = \alpha \frac{d_w^I}{d_{iris}^I} \cdot \{x_i^F\}_{i=1}^N \tag{5}$$

Metric Headpose With metric facial landmarks, we estimate the 3D metric transformation matrix $P = [R \mid t']$ representing head pose. The rotation matrix R from MediaPipe's relative pose output $P = [R \mid t]$, is scale-invariant and can be reused to estimate the metric translation t'. We propose an iterative refinement algorithm based on our novel radial Procrustes alignment (Gower 1975) and similar triangles. The goal is to minimize the Euclidean distance between the original UVZ landmarks and the newly projected 3D landmarks under the estimated transformation:

$$t' = \arg\min_{t'} \sum_{i=1}^{N} \|x_i^I - K \cdot [R \mid t'] \cdot x_i^{F'}\|^2 \tag{6}$$

The algorithm initializes with depth $z_0 = 60$ cm, based on average monitor-to-face distance reported in (Cheng et al. 2021), and an initial XY estimate derived by reprojecting the nose's UV position. This step aligns the UV center of projected and original UVZ points, reducing the problem to iterative depth refinement. A lightweight radial Procrustes method determines the direction and magnitude of the depth update by computing a unit direction vector v_i from the center c between matched projected points $\hat{x}_i^I$ and original landmarks x_i^I, using:

$$v_i = \frac{x_i^I - \hat{x}_i^I}{\|x_i^I - \hat{x}_i^I\|} \tag{7}$$

$$z_{\text{update}} = \text{clip}\left(\frac{\beta}{N}\sum_{i=1}^{N} \text{sign}(v_i \cdot c_i) \cdot \|v_i\|, -\Delta_{\max}, \Delta_{\max}\right), \tag{8}$$

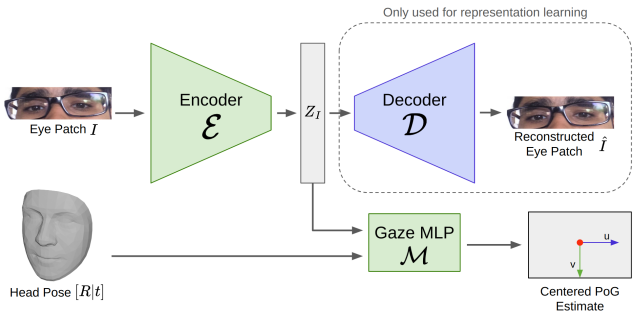

Figure 4: **BlazeGaze Architecture**: The BlazeGaze model takes as input the eye patch and the metric head pose and is composed of BlazeBlock-based encoder, decoder, and a gaze multi-layer perceptron (MLP). The decoder is used in representation learning, but is discarded during meta-learning.

where β is a scaling factor of 0.1 and $\Delta_{\max}$ is a threshold cap of 5 cm. A clip function acts as safety guardrails.

After computing and applying z_{update}, the corresponding metric XY values are updated via similar triangles to preserve the reprojection consistency, ensuring the projected nose center $\hat{x}_{\text{nose}}^I$ aligns with the observed nose center $\hat{x}_{\text{nose}}^I$. The iterative algorithm stops when $z_{\text{update}} < 0.25$ cm or when the iteration cap of 10 is reached.

3.2 BlazeGaze: Lightweight Personalized Gaze

As shown in Fig. 4, BlazeGaze consists of an encoder $\mathcal{E} : I \to \mathbf{z}$, decoder $\mathcal{D} : \mathbf{z} \to \hat{I}$, and gaze estimator $\mathcal{M} : (\mathbf{z}, [R \mid t]) \to \mathbf{g}$. We adopt a two-stage training strategy (see Fig. 2). In Stage 1, all components are trained jointly to learn a robust embedding via a standard train/validation split. In Stage 2, the decoder is discarded, the encoder is frozen, and the gaze estimator is adapted into a meta-learner using MAML to enable efficient user adaptation. This separation reduces the number of trainable parameters during meta-learning and avoids instability from joint optimization. To enhance cross-device generalization (e.g., mobile in GazeCapture vs. laptops in MPIIFaceGaze), gaze predictions are normalized to $\mathbf{g} \in [[-0.5, 0.5]]^2$ with the origin at screen center, enabling device-agnostic evaluation across varying screen resolutions and sizes.

Gaze-Aware Representation Learning The first-stage of training uses a multi-objective loss function defined as:

$$\mathcal{L}_{\text{all}} = \beta_{\text{r}}\mathcal{L}_{\text{r}} + \beta_{\text{g}}\mathcal{L}_{\text{g}} + \beta_{\text{c}}\mathcal{L}_{\text{c}}, \tag{9}$$

where $\beta = \{\beta_r, \beta_g, \beta_c\}$ have been empirically determine for each dataset, with initial parameters inspired from Park et al. (2019). These loss functions are explain in the following paragraphs.

Image Reconstruction. We train the encoder-decoder using a standard pixel-wise reconstruction loss that minimizes the mean squared error (MSE) between the input image I and its reconstruction $\hat{I}$:

$$\mathcal{L}_{\text{r}}(I, \hat{I}) = \frac{1}{|I|} \sum_{u \in I, \hat{u} \in \hat{I}} (u - \hat{u})^2, \tag{10}$$

where u and $\hat{u}$ represent individual pixel values in the original and reconstructed images, respectively. This training objective encourages the encoder to learn a compact latent space that captures the essential visual structures of the eye region, including features relevant to gaze direction.

Weighted L2 Loss for 2D PoG Estimation. Given ground truth gaze positions $\mathbf{g}_{\text{true}}$ and predicted values $\mathbf{g}_{\text{pred}}$, we compute the weighted L2 loss as:

$$\mathcal{L}_{\text{g}} = \frac{1}{B} \sum_{i=1}^{B} w_i \left\| \mathbf{g}_{\text{pred}}^{(i)} - \mathbf{g}_{\text{true}}^{(i)} \right\|^2, \tag{11}$$

where B is the batch size and w_i is the scalar weight for sample i. The weight is obtained from a precomputed 30×30 grid of inverse frequency for each dataset to address ground truth region imbalance. Additional details about sample weights are provided in the supplementary materials.

Embedding Consistency Loss. To encourage gaze-consistent embeddings, we define a contrastive-style loss that aligns pairwise distances in embedding space with pairwise distances in normalized 2D gaze space.

We first compute the normalized Euclidean distance δ_{ij} between the PoG gaze $\mathbf{g}$:

$$\delta_{ij} = \frac{\|\mathbf{g}_i - \mathbf{g}_j\|_2}{\max_{i,j} \|\mathbf{g}_i - \mathbf{g}_j\|_2 + \varepsilon} \tag{12}$$

where ε is a small constant for numerical stability.

Then, the loss is defined as:

$$\mathcal{L}_{\text{c}} = \frac{1}{B^2} \sum_{i=1}^{B} \sum_{j=1}^{B} w_{ij} \left(\|\mathbf{z}_i - \mathbf{z}_j\|_2 - \delta_{ij} \right)^2, \tag{13}$$

where z_i, z_j are corresponding latent embeddings. This loss penalizes discrepancies between the relative distances in embedding space and the normalized distances in PoG space. The goal is to structure the embedding space such that its geometry reflects gaze similarity, thereby improving downstream generalization and calibration. Additional discussion on the effectiveness of gaze-based loss functions is provided in the supplementary material.

Adaptable Gaze Estimator To enable rapid personalization with minimal calibration, we adopt a MAML framework to train a gaze estimator $\mathcal{M}_\theta$ that quickly adapts to new users. The goal is to learn meta-parameters θ^* such that, with only a few gradient steps on a small calibration set, the model performs well on unseen users.

We frame gaze estimation as a distribution over tasks, each representing gaze prediction for an individual. Each task comprises a small support set ($k \leq 9$) and a corresponding query set from the same participant. Training minimizes post-adaptation validation loss, encouraging generalization to new users rather than overfitting to training data.

Let $\mathcal{S}_{\text{train}}$ and $\mathcal{S}_{\text{test}}$ denote disjoint sets of users for meta-training and meta-testing. In each training iteration, a user $P_i \in \mathcal{S}_{\text{train}}$ is sampled, and a task $\mathcal{T}_i = \{\mathcal{D}_i^{\text{s}}, \mathcal{D}_i^{\text{q}}\}$ is constructed. The support set $\mathcal{D}_i^{\text{s}} = \{(\mathbf{z}_j, \mathbf{h}_j, \mathbf{g}_j, w_j)\}_{j=1}^{k}$ includes latent embeddings, head poses $\mathbf{h}_j = [R_j \mid t_j]$, 2D gaze targets, and sample weights. The query set $\mathcal{D}_i^{\text{q}}$ contains l additional samples from the same user.

From initial model parameters θ, we compute task-adapted weights θ_i' via gradient descent on the support set:

$$\theta_i' = \theta - \alpha \nabla_\theta \mathcal{L}_g^i(\theta), \tag{14}$$

where α is the inner-loop learning rate and $\mathcal{L}_g^i$ is the weighted L2 gaze loss. The adapted model is then evaluated on $\mathcal{D}_i^{\text{q}}$, producing the meta-loss:

$$\mathcal{L}_{\text{meta}} = \sum_i \mathcal{L}_g^i(\theta_i'). \tag{15}$$

Meta-gradients update the initialization via:

$$\theta \leftarrow \theta - \eta \nabla_\theta \mathcal{L}_{\text{meta}}, \tag{16}$$

with η as the outer-loop learning rate. This process is repeated across tasks to learn the meta-initialization θ^*.

At test time, given a new user $P_{\text{test}} \in \mathcal{S}_{\text{test}}$ and support set $\mathcal{D}_{\text{test}}^{\text{s}}$, we adapt θ^* using:

$$\theta_{\text{test}} = \theta^* - \alpha \nabla_\theta \mathcal{L}_g^{\text{test}}(\theta^*), \tag{17}$$

yielding a personalized model $\mathcal{M}_{\theta_{\text{test}}}$ evaluated on a held-out query set. This allows effective adaptation from as few as $k \leq 9$ samples, enabling low-effort personalization suitable for real-time, in-browser, and mobile settings.

4 Implementation

4.1 Data Preprocessing

Our normalization pipeline is tailored for browser-based deployment, where iterative Perspective-n-Point (PnP) solvers and camera intrinsics are unavailable. Instead of using PnP, we compute a homography transformation using the facial landmarks computed by the MediaPipe Facial Landmark Detection model to warp the eye region such that the head appears upright and centered.

4.2 Neural Networks

Encoder. The encoder $\mathcal{E}$ uses a combination of single and double BlazeBlocks for efficient feature extraction from $(128 \times 512 \times 3)$ eye-region images. It outputs a latent embedding of shape (512).

Decoder. The decoder $\mathcal{D}$ mirrors the encoder structure, using Conv2DTranspose layers to reconstruct the input image.

Gaze Estimator. The gaze model $\mathcal{M}$ takes the gaze embedding and auxiliary head pose as inputs and propagates their values through a 3-layer multilayer perceptron (MLP) of sizes 16, 16, and 2.

Table 1: **Gaze Estimation Benchmark Across Accuracy and Efficiency Metrics.** PoG error (cm) on MPIIFaceGaze ($\mathcal{D}_{\text{M}}$), GazeCapture ($\mathcal{D}_{\text{G}}$), and EyeDiap ($\mathcal{D}_{\text{E}}$), reported alongside GFLOPs, parameter count (M), inference delay (ms), and frame per second (FPS). Lower is better for all metrics except FPS. **Bold** indicates best performance.

Methods	Year	Open	$\mathcal{D}_{\text{M}} \downarrow$	$\mathcal{D}_{\text{G}} \downarrow$	$\mathcal{D}_{\text{E}} \downarrow$	GFLOPs $\downarrow$	#MParams $\downarrow$	Delay $\downarrow$	FPS $\uparrow$
Mnist	2015	Yes	7.29	NA	9.06	0.10	1.82	3.13	319.0
iTracker	2016	Yes	7.67	2.81	10.13	3.97	6.28	33.33	30.0
GazeNet	2017	Yes	6.62	NA	8.51	72.24	90.23	246.31	4.1
FullFace	2017	Yes	5.65	NA	7.70	29.90	190	174.55	5.7
RT-Gene	2018	Yes	5.36	NA	7.19	12.21	31.66	43.48	23.0
SAGE	2019	No	NA	2.72	NA	**0.04**	NA	NA	NA
TAT	2019	No	NA	2.66	NA	NA	NA	NA	NA
DilatedNet	2019	Yes	5.07	NA	7.36	202	3.92	1207.73	0.8
Gaze360	2019	Yes	4.66	NA	6.37	3.65	11.94	24.39	41.0
CA-Net	2020	No	4.90	NA	**6.30**	NA	NA	NA	NA
AFF-Net	2021	Yes	4.21	**2.30**	9.25	26.14	1.94	109.81	9.1
EFE	2023	No	**3.89**	2.48	NA	17.51	120	1818.18	0.6
BlazeGaze	2025	Yes	4.56	2.32	7.53	0.15	**0.16**	**0.88**	**1137.0**

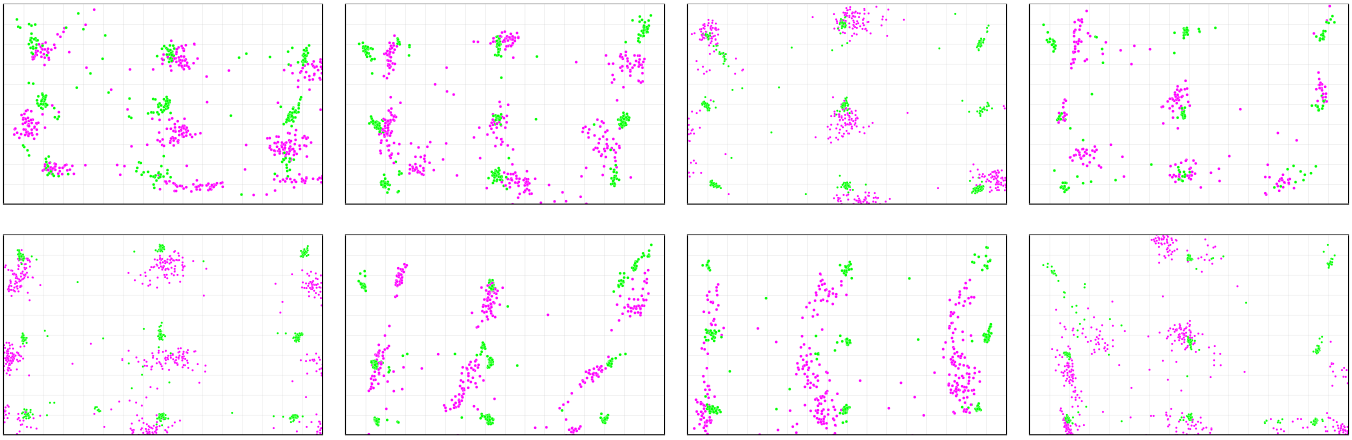

Figure 5: **Qualitative Comparison:** Predicted gaze points from WEBEYETRACK (magenta) vs. ground truth from Tobii X3-120 (green) during the final Dot Test in the Eye of the Typer dataset.

4.3 Training

Representation Learning. BlazeGaze is first trained to map inputs to a gaze-aware embedding space. Training runs for 20 epochs with a batch size of 8, using Adam optimizer and exponential learning rate decay 1×10^{-3} and a decay rate of 0.95. The best model is saved, the decoder is discarded, and the encoder is frozen for meta-learning.

Meta-learning. After learning the representation space, we apply first-order MAML to train $\mathcal{M}$ for rapid personalization. Tasks are defined per user with $k = 9$ support and $l = 100$ query samples. Inner-loop updates use SGD with $\alpha = 1 \times 10^{-5}$; the outer loop uses Adam with $\eta = 1 \times 10^{-3}$, trained for 1000 steps with 5 inner updates per task.

Deployment. All components are initially implemented and trained in Python and TensorFlow 2. The trained models are then converted using `tensorflowjs_converter`. The JavaScript version of the framework utilizes TensorFlow.js, specifically the `LayerModels` API[2] to support on-device model training and ensure user data never leaves the device.

5 Experiments

We demonstrate the effectiveness and real-world capabilities of WEBEYETRACK across image and video gaze datasets, illustrating the feasibility of developing SOTA gaze estimation solutions that are compatible with consumer-grade hardware, as our proposed framework achieves competitive accuracy while maintaining minimal computational overhead.

5.1 Datasets

We evaluate WEBEYETRACK on four public datasets covering mobile, webcam, and lab-based scenarios, with con-

[2]https://js.tensorflow.org/api/latest/#class:LayersModel

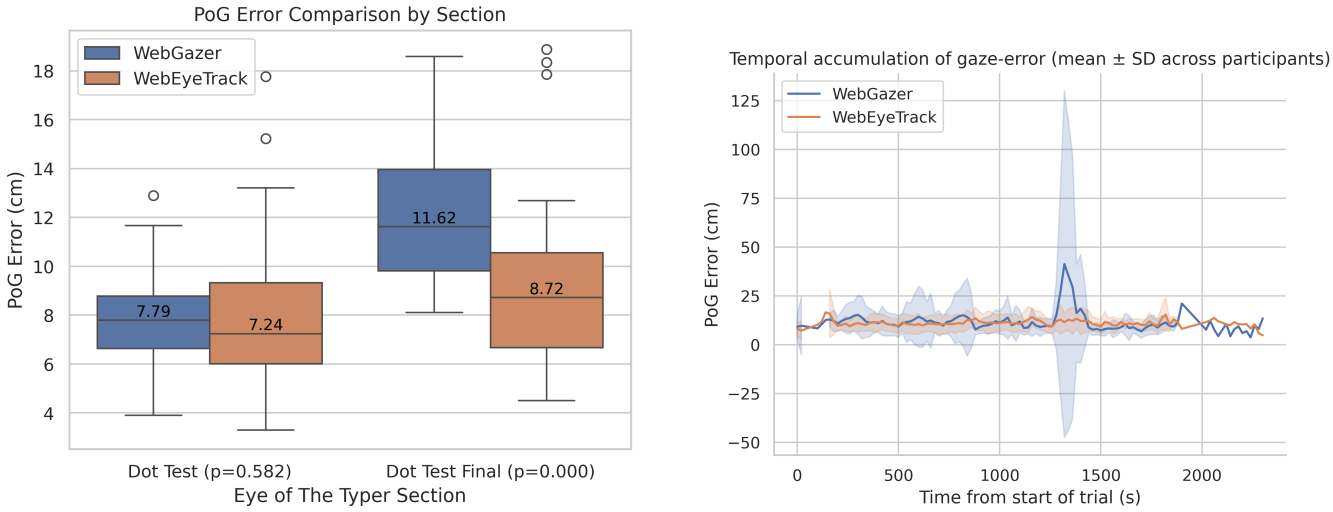

Figure 6: **Temporal Accuracy Analysis:** Beginning vs. end accuracy illustrating gaze drift in a 20-minute session (**left**). Average PoG error over time for WEBEYETRACK and WebGazer, with mean and standard deviation across participants (**right**).

sistent preprocessing and normalization for comparability (Park et al. 2019; Balim et al. 2023).

GazeCapture Crowdsourced on iOS, >2.5M frames from 1450+ users, with screen coordinates normalized via device metadata.

MPIIFaceGaze Webcam data from 15 subjects (∼3000 frames each) under varied conditions; gaze points normalized to screen dimensions.

EyeDiap Lab dataset with 16 participants; HD camera footage used with normalized gaze labels.

Eye of the Typer Tobii Pro X3-120 (120 Hz) eye-tracking during web tasks; we use the "Dot Test" segments with authors' synchronized preprocessing.

5.2 Results

We evaluate WEBEYETRACK in two settings: (1) within-dataset performance on standard image-based gaze datasets (MPIIFaceGaze, GazeCapture, EyeDiap), and (2) cross-dataset generalization to the Eye of the Typer video dataset. The first setting assesses accuracy and efficiency against SOTA gaze models, while the second compares WEBEYETRACK directly to the leading browser-based solution, WebGazer, under real-world conditions.

Within-Dataset Accuracy vs. Inference Time We perform two-stage training on each dataset and report the resulting PoG error and computational performance in Figure 1 and Table 1. All inference metrics were computed using a 11th Gen Intel (R) Core(TM) i7-11700F @ 2.50Ghz CPU.

BlazeGaze achieves accuracy comparable to modern, compute-intensive models, while significantly improving runtime efficiency. Notable, it outperforms the previous fastest model (Mnist) with a 256% increase in FPS. These results highlights a growing trend in the field: recent models tend to prioritize large architectures (e.g., CNNs, ViTs), often sacrificing real-time viability. In contrast, BlazeGaze offers an effective trade-off between accuracy and speed (see Fig. 1), making it suitable for real-world deployment. Additional runtime benchmarks on laptops and mobile devices are provided in the supplementary material.

5.3 Cross-Dataset Evaluation: Eye of the Typer

To test generalization, we evaluate BlazeGaze trained on MPIIFaceGaze against the Eye of the Typer dataset to measure the model's robustness to temporal and unseen person gaze estimation. The dataset includes five activities per session: 3×3 Dot Tests at the beginning and end for calibration and evaluation, and intermediate tasks involving typing and reading. WEBEYETRACK is calibrated per participant using only the initial Dot Test (9-point grid).

Qualitative Gaze Visualizations While most gaze benchmarks rely on single-frame image datasets, temporal consistency is rarely assessed. In Fig. 5, we visualize gaze predictions from the final Dot Test. Despite 20-minute sessions, WEBEYETRACK's predicted gaze points remain closely aligned with ground truth from the Tobii eye-tracker, demonstrating strong spatial and temporal consistency.

Temporal Accuracy and Degradation Fig. 6 shows the change in L1 PoG error between the initial and final Dot Tests. WebGazer's error rises 49% (7.79 cm→ 11.62 cm), while WEBEYETRACK increases only 20% (7.24 cm → 8.72 cm). A Mann–Whitney U test confirms that WebEyeTrack's final error is significantly lower ($p < 0.05$), indicating better robustness to temporal drift.

WebGazer's larger drop stems from its reliance on click-based recalibration, which lacks head-pose modeling and fails during uninterrupted tasks like typing. As shown in

Fig. 6, PoG error over time (10s windows) reveals WebGazer's mid-session instability, while WEBEYETRACK maintains lower variance and greater temporal stability.

6 Conclusion

We presented WEBEYETRACK, a real-time, browser-compatible gaze estimation framework that integrates metric head pose estimation with few-shot personalization. By combining lightweight representation learning, meta-learning, and efficient in-browser execution, WEBEYETRACK achieves competitive accuracy with low computational overhead, making it suitable for deployment on consumer devices. Evaluations across multiple datasets demonstrate robust performance across users and time. Future work includes improving model fairness and reducing energy consumption.

7 Acknowledgments

The research reported here was supported by the Institute of Education Sciences, U.S. Department of Education, through Grant R305A150199 and R305A210347 to Vanderbilt University. The opinions expressed are those of the authors and do not represent views of the Institute or the U.S. Department of Education.

References

Alberto Funes Mora, K.; Monay, F.; and Odobez, J.-M. 2014. EYEDIAP: A Database for the Development and Evaluation of Gaze Estimation Algorithms from RGB and RGB-D Cameras.

Balim, H.; Park, S.; Wang, X.; Zhang, X.; and Hilliges, O. 2023. EFE: End-to-end Frame-to-Gaze Estimation. *IEEE Computer Society Conference on Computer Vision and Pattern Recognition Workshops*, 2023-June: 2688–2697. ISBN: 9798350302493.

Baltrusaitis, T.; Zadeh, A.; Lim, Y. C.; and Morency, L.-P. 2018. OpenFace 2.0: Facial Behavior Analysis Toolkit. In *2018 13th IEEE International Conference on Automatic Face & Gesture Recognition (FG 2018)*, 59–66. Xi'an: IEEE. ISBN 978-1-5386-2335-0.

Bazarevsky, V.; Kartynnik, Y.; Vakunov, A.; Raveendran, K.; and Grundmann, M. 2019. BlazeFace: Sub-millisecond Neural Face Detection on Mobile GPUs. ArXiv:1907.05047 [cs].

Brousseau, B.; Rose, J.; and Eizenman, M. 2018. Accurate Model-Based Point of Gaze Estimation on Mobile Devices. *Vision*, 2(3): 35.

Cheng, Y.; and Lu, F. 2022. Gaze Estimation using Transformer. In *2022 26th International Conference on Pattern Recognition (ICPR)*, 3341–3347. Montreal, QC, Canada: IEEE. ISBN 978-1-6654-9062-7.

Cheng, Y.; Lu, F.; and Zhang, X. 2018. Appearance-Based Gaze Estimation via Evaluation-Guided Asymmetric Regression. In Ferrari, V.; Hebert, M.; Sminchisescu, C.; and Weiss, Y., eds., *Computer Vision – ECCV 2018*, volume 11218, 105–121. Cham: Springer International Publishing. ISBN 978-3-030-01263-2 978-3-030-01264-9. Series Title: Lecture Notes in Computer Science.

Cheng, Y.; Wang, H.; Bao, Y.; and Lu, F. 2021. Appearance-based Gaze Estimation With Deep Learning: A Review and Benchmark. 14(8): 1–20.

Dongheng Li; Winfield, D.; and Parkhurst, D. 2005. Starburst: A hybrid algorithm for video-based eye tracking combining feature-based and model-based approaches. In *2005 IEEE Computer Society Conference on Computer Vision and Pattern Recognition (CVPR'05) - Workshops*, volume 3, 79–79. San Diego, CA, USA: IEEE. ISBN 978-0-7695-2372-9.

Gower, J. C. 1975. Generalized Procrustes Analysis. *Psychometrika*, 40(1): 33–51.

Grishchenko, I.; Ablavatski, A.; Kartynnik, Y.; Raveendran, K.; and Grundmann, M. 2020. Attention Mesh: High-fidelity Face Mesh Prediction in Real-time.

Guo, J.; Zhu, X.; Yang, Y.; Yang, F.; Lei, Z.; and Li, S. Z. 2021. Towards Fast, Accurate and Stable 3D Dense Face Alignment. ArXiv:2009.09960 [cs].

He, J.; Pham, K.; Valliappan, N.; Xu, P.; Roberts, C.; Lagun, D.; and Navalpakkam, V. 2019. On-Device Few-Shot Personalization for Real-Time Gaze Estimation. In *2019 IEEE/CVF International Conference on Computer Vision Workshop (ICCVW)*, 1149–1158. Seoul, Korea (South): IEEE. ISBN 978-1-7281-5023-9.

Heck, M.; Becker, C.; and Deutscher, V. 2023. Webcam Eye Tracking for Desktop and Mobile Devices: A Systematic Review. Hawaii, USA. ISBN 978-0-9981331-6-4.

Huynh, S.; Balan, R. K.; and Ko, J. 2021. iMon: Appearance-based Gaze Tracking System on Mobile Devices. *Proceedings of the ACM on Interactive, Mobile, Wearable and Ubiquitous Technologies*, 5(4): 1–26.

iMotions. 2023. iMotions WebET 3.0: Webcam Based Eye Tracking - Whitepaper v3.

Jacob, R. J. K.; and Karn, K. S. 2003. Commentary on Section 4 - Eye Tracking in Human-Computer Interaction and Usability Research: Ready to Deliver the Promises. In Hyönä, J.; Radach, R.; and Deubel, H., eds., *The Mind's Eye*, 573–605. Amsterdam: North-Holland. ISBN 978-0-444-51020-4.

Kazemi, V.; and Sullivan, J. 2014. One millisecond face alignment with an ensemble of regression trees. In *2014 IEEE Conference on Computer Vision and Pattern Recognition*, 1867–1874. Columbus, OH: IEEE. ISBN 978-1-4799-5118-5.

Krafka, K.; Khosla, A.; Kellnhofer, P.; Kannan, H.; Bhandarkar, S.; Matusik, W.; and Torralba, A. 2016. Eye Tracking for Everyone.

Li, Y.; Zhan, Y.; and Yang, Z. 2020. Evaluation of appearance-based eye tracking calibration data selection. In *2020 IEEE International Conference on Artificial Intelligence and Computer Applications (ICAICA)*, 222–224. Dalian, China: IEEE. ISBN 978-1-7281-7005-3.

Papoutsaki, A.; Daskalova, N.; Sangkloy, P.; Huang, J.; Laskey, J.; and Hays, J. 2016. WebGazer: Scalable Webcam Eye Tracking Using User Interactions. New York City, USA.

Papoutsaki, A.; Gokaslan, A.; Tompkin, J.; He, Y.; and Huang, J. 2018. The eye of the typer: A benchmark and analysis of gaze behavior during typing. In *Eye Tracking Research and Applications Symposium (ETRA)*. Association for Computing Machinery. ISBN 978-1-4503-5706-7.

Park, J.; Park, S.; and Cha, H. 2021. GAZEL: Runtime Gaze Tracking for Smartphones. In *2021 IEEE International Conference on Pervasive Computing and Communications (PerCom)*, 1–10. Kassel, Germany: IEEE. ISBN 978-1-6654-0418-1.

Park, S.; Mello, S. D.; Molchanov, P.; Iqbal, U.; Hilliges, O.; and Kautz, J. 2019. Few-Shot Adaptive Gaze Estimation. In *2019 IEEE/CVF International Conference on Computer Vision (ICCV)*, 9367–9376. Seoul, Korea (South): IEEE. ISBN 978-1-7281-4803-8.

Pietrzak, M.; Duchowski, A.; Krejtz, I.; Krejtz, K.; Zarnowiec, F.; and Sromek, D. 2025. RealEye Webcam Eye-Tracking for Computers Technology White Paper.

Shukla, D. K.; Maurya, A.; Pal, M.; and Shivahare, B. D. 2023. A Survey on Exploring the Evolution and Trends of Web Development.

Soukupová, T. 2016. Real-Time Eye Blink Detection using Facial Landmarks.

Sugano, Y.; Matsushita, Y.; and Sato, Y. 2014. Learning-by-Synthesis for Appearance-Based 3D Gaze Estimation. In *2014 IEEE Conference on Computer Vision and Pattern Recognition*, 1821–1828. Columbus, OH, USA: IEEE. ISBN 978-1-4799-5118-5.

Wang, K.; and Ji, Q. 2017. Real Time Eye Gaze Tracking with 3D Deformable Eye-Face Model. In *Proceedings of the IEEE International Conference on Computer Vision*, volume 2017-October, 1003–1011. Institute of Electrical and Electronics Engineers Inc. ISBN 978-1-5386-1032-9. ISSN: 15505499.

Wen, Q.; Bradley, D.; Beeler, T.; Park, S.; Hilliges, O.; Yong, J.; and Xu, F. 2020. Accurate Real-time 3D Gaze Tracking Using a Lightweight Eyeball Calibration Rights / license: Creative Commons Attribution 4.0 International Accurate Real-time 3D Gaze Tracking Using a Lightweight Eyeball Calibration. 39(2).

Wood, E.; and Bulling, A. 2014. EyeTab: model-based gaze estimation on unmodified tablet computers. In *Proceedings of the Symposium on Eye Tracking Research and Applications*, 207–210. Safety Harbor Florida: ACM. ISBN 978-1-4503-2751-0.

Xu, P.; Ehinger, K. A.; Zhang, Y.; Finkelstein, A.; Kulkarni, S. R.; and Xiao, J. 2015. TurkerGaze: Crowdsourcing Saliency with Webcam based Eye Tracking.

Yu, Y.; Liu, G.; and Odobez, J.-M. 2019. Deep Multitask Gaze Estimation with a Constrained Landmark-Gaze Model. In Leal-Taixé, L.; and Roth, S., eds., *Computer Vision – ECCV 2018 Workshops*, volume 11130, 456–474. Cham: Springer International Publishing. ISBN 978-3-030-11011-6 978-3-030-11012-3. Series Title: Lecture Notes in Computer Science.

Zhang, X.; Sugano, Y.; and Bulling, A. 2018. Revisiting data normalization for appearance-based gaze estimation. In *Eye Tracking Research and Applications Symposium (ETRA)*. Association for Computing Machinery. ISBN 978-1-4503-5706-7.

Zhang, X.; Sugano, Y.; and Bulling, A. 2019. Evaluation of appearance-based methods and implications for gaze-based applications. In *Conference on Human Factors in Computing Systems - Proceedings*. Association for Computing Machinery. ISBN 978-1-4503-5970-2.

Zhang, X.; Sugano, Y.; Fritz, M.; and Bulling, A. 2015. Appearance-Based Gaze Estimation in the Wild.

Zhang, X.; Sugano, Y.; Fritz, M.; and Bulling, A. 2016. It's Written All Over Your Face: Full-Face Appearance-Based Gaze Estimation.